

Deformable Mamba for Wide Field of View Segmentation

Jie Hu^{1,*}, Junwei Zheng^{1,*}, Jiale Wei¹, Jiaming Zhang^{1,2,†}, Rainer Stiefelhagen¹

¹Karlsruhe Institute of Technology, ²ETH Zurich

<https://github.com/JieHu1996/DeformableMamba>

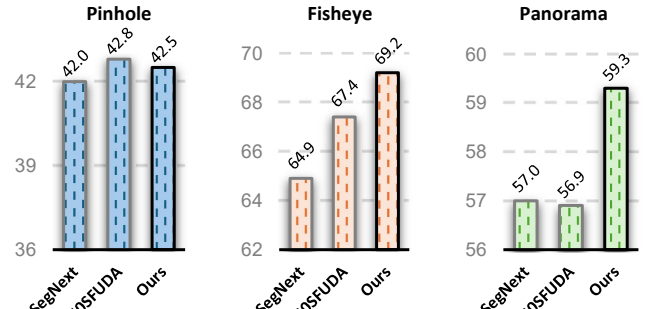
Abstract

Recent advancements in the Mamba architecture, with its linear computational complexity, being a promising alternative to transformer architectures suffering from quadratic complexity. While existing works primarily focus on adapting Mamba as vision encoders, the critical role of task-specific Mamba decoders remains under-explored, particularly for distortion-prone dense prediction tasks. This paper addresses two interconnected challenges: (1) The design of a Mamba-based decoder that seamlessly adapts to various architectures (e.g., CNN-, Transformer-, and Mamba-based backbones), and (2) The performance degradation in decoders lacking distortion-aware capability when processing wide-FoV images (e.g., 180° fisheye and 360° panoramic settings). We propose the Deformable Mamba Decoder, an efficient distortion-aware decoder that integrates Mamba’s computational efficiency with adaptive distortion awareness. Comprehensive experiments on five wide-FoV segmentation benchmarks validate its effectiveness. Notably, our decoder achieves a +2.5% performance improvement on the 360° Stanford2D3D segmentation benchmark while reducing 72% parameters and 97% FLOPs, as compared to the widely-used decoder heads.

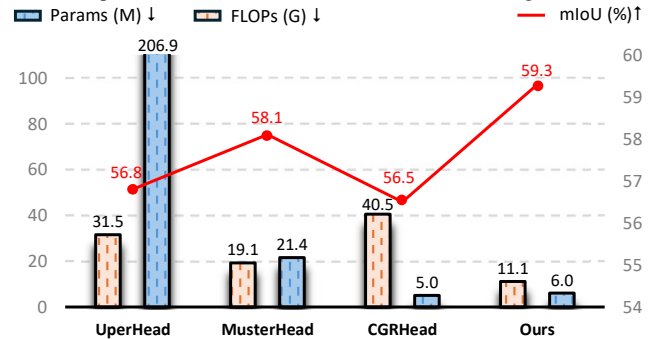
1. Introduction

Dense image analysis like image segmentation [2, 20, 55] is a fundamental task in computer vision, forming a crucial component of numerous downstream vision-based applications [67]. At the same time, advancements in sensor technology have led to a variety of sensor types, each with unique characteristics that impact imaging. In recent years, diverse sensors such as pinhole cameras, fisheye cameras [45, 62] with 180° field of views (FoV), and even panoramic cameras [1, 3, 65] with 360° FoV have been increasingly adopted across vision tasks.

Based on our experiments (Fig. 1a), we observe that directly applying models designed for narrow-FoV data to



(a) Comparison across narrow- and wide-FoV semantic segmentation.



(b) Performance and efficiency comparison of different decoders on Stanford2D3D [1] panoramic dataset with the same backbone [34].

Figure 1. Our deformable Mamba (a) achieves better results across wide-FoV semantic segmentation while (b) maintaining parameter and computational efficiency.

wide-FoV data often leads to a suboptimal solution. For instance, SegNext [20] specifically designed for narrow-FoV pinhole cameras typically cannot generalize well when used for analyzing fisheye images with 180° FoV or panoramic images with 360° FoV. This is primarily due to the high degree of image distortion and object deformation present in wide-FoV cameras. As shown in Fig. 2, the altered pixel arrangement in wide-FoV images might lead to misclassifications and limits adaptability of narrow-FoV models [2, 5, 7, 47, 69]. To address this, previous methods have spent a large effort in architecture design to fit specific sensor types, such as CNN-based and transformer-based models [29, 49] for fisheye images, as well as approaches [64, 65] tailored to mitigate distortion in panoramic segmentation.

*Equal contribution.

†Corresponding author (e-mail: jiaming.zhang@kit.edu).

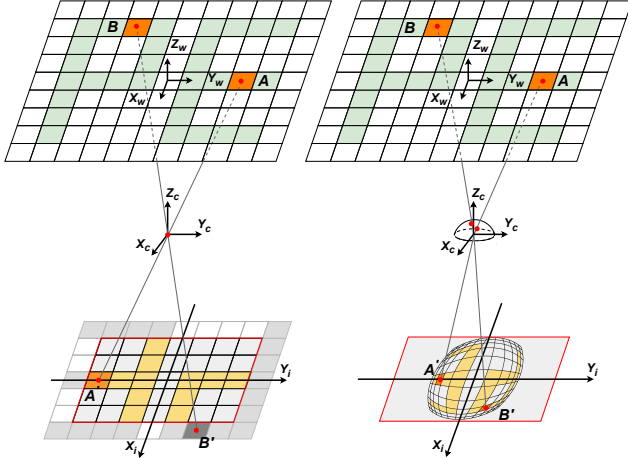


Figure 2. Comparison of camera imaging with narrow-FoV (left) and wide-FoV (right) cameras. Narrow-FoV cameras maintain geometric fidelity but limited coverage, whereas wide-FoV cameras offer expansive scene capture while introducing substantial geometric distortions.

However, most existing methods deeply couple distortion-aware capability with the entire model (both encoder and decoder). The drawbacks are two-fold: (1) These models are often designed for specific FoVs, yet hard to adapt to varying distortion characteristics. For example, narrow-FoV model SegNext [20] and wide-FoV model 360SFUDA [70] cannot consistently perform well across different wide-FoV segmentation (Fig. 1a).

(2) The tight coupling with the overall architecture limits the reusability of large-scale pretrained backbones, as any modification requires retraining. Therefore, in this work, we focus on flexible decoder designs and constrain distortion awareness to the decoder level, yielding greater flexibility in utilizing diverse pretrained backbones, striking a tradeoff between adaptability and modularity.

Furthermore, we mainly utilize the Mamba [17] mechanism due to its benefit of linear computational complexity. However, most previous works [4, 24, 30, 34, 58, 72, 73] have focused on Mamba-based encoders, research on corresponding decoders for downstream tasks remains limited. We contend that decoders are equally crucial as encoders in the context of dense prediction tasks. As illustrated in Fig. 1b, a widely used decoder UperHead [54] excels at multi-scale feature fusion but suffers from excessive computational overhead. Alternative methods [38, 57] applied lightweight CNN- and transformer-based decoders to reduce computational cost. However, they suffer notable performance degradation when processing wide-FoV data.

To address these challenges, we propose the **Deformable Mamba Decoder**, an efficient distortion-aware decoder for image segmentation across varying wide-FoVs. In this work, a unified framework is created to effectively handling images from multiple camera types and sources,

spanning FoVs from 180° to 360° , from indoor to outdoor scenarios, in synthetic and real-world imageries. Our deformable decoder can seamlessly integrate with CNN-, transformer-, and Mamba-based backbones, imparting distortion-awareness capability to the overall model.

To evaluate the effectiveness of our method, we conduct extensive experiments across five datasets for wide-FoV segmentation, including two 180° (WoodScape [62], SynWoodScape [45]) datasets and three 360° (Stanford2D3D [1], Matterport3D [3], SynPASS [65]). Our framework performs consistently well across various datasets. Notably, while reducing the decoder parameters by 72% and FLOPs by 97%, Deformable Mamba achieved state-of-the-art performance, with a +2.5% absolute improvement over previous VMamba [34] on the 360° Stanford2D3D dataset. To summarize, our contributions are as follows.

- We propose an efficient decoder based on the Mamba architecture, which addresses the gap in decoder-oriented Mamba-based efficient approaches.
- For the first time, we incorporate distortion-awareness exclusively at the Mamba decoder level, decoupling it from the overall framework, which enables integration with CNN-, Transformer-, and Mamba-based backbones to enhance distortion perception.
- Extensive experiments on five datasets across a variety of indoor and outdoor, synthetic and real-world wide-FoV scenes, demonstrate the state-of-the-art performance of our method in wide-FoV segmentation.

2. Related Work

2.1. Wide Field of View Segmentation

Wide-FoV image segmentation has received increasing attention as it enables broader scene understanding in applications such as autonomous driving and robotics. Wide-FoV images, like panoramic and fisheye images, offer expansive visual coverage but introduce unique challenges due to geometric distortions, spatial resolution variations, and uneven feature distribution. Early segmentation methods [2, 5, 6, 10, 16, 18, 25, 32, 33, 36, 47, 55, 63, 63, 67, 69] have achieved significant success on narrow-FoV image segmentation. However, directly applying pinhole models to wide-FoV images often results in downgraded performance due to object deformations and image distortions. Previous work [59, 60] propose the Panoramic Annular Semantic Segmentation (PASS) framework using a panoramic annular lens system. [26] introduces panoramic panoptic segmentation for panoramic views. In [64, 65], deformable modules are proposed to enhance the distortion perception capability in transformers. Zheng *et al.* [68] introduce the Open Panoramic Segmentation (OPS) task in an open-vocabulary context. Apart from panoramas, pre-

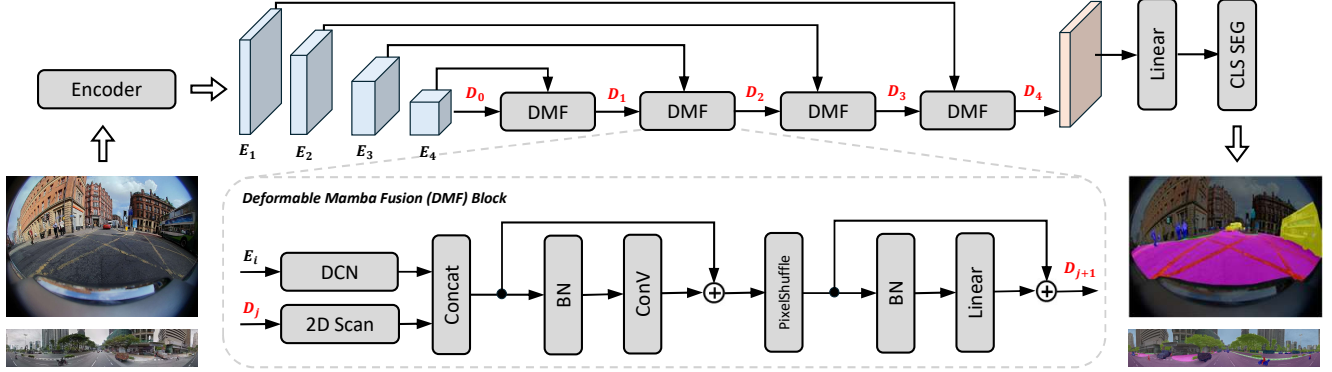


Figure 3. Overview of the Deformable Mamba (DMamba) framework. Given wide-FoV images (180° or 360°), the features extracted by an encoder, are fused by the proposed Deformable Mamba Decoder, which constructed by four Deformable Mamba Fusion (DMF) modules.

vious methods [12, 29] revolve around multi-task on fish-eye images, while a pretraining paradigm [39] and semi-supervised approaches [40, 42] are introduced to address the challenges of fisheye data. Manzoor *et al.* [37] substitutes the conventional convolutional modules in U-Net [44] and residual U-Net [43] with restricted deformable convolution (RDC) [12], imparting fisheye-distortion awareness to the model. Departing from these approaches, we are the first to propose a unified model applicable to all wide-FoV inputs, including panoramic and fisheye images.

2.2. Vision Mambas

CNN [28] have achieved notable success in computer vision with efficient local feature extraction and hierarchical learning, while Transformer [51] excel at modeling long-range dependencies despite their quadratic complexity. Recently, the state-space-model (SSM)-based Mamba [17] architecture has emerged as a promising alternative, offering linear complexity and parallel computation through its selective scan mechanism, enabling efficient long-sequence modeling. The application of Mamba in sequence modeling has naturally extended to vision tasks. The serialized processing of input tokens in the Mamba architecture presents notable challenges when transferring to vision tasks. Zhu *et al.* [72] serialize the image using patch embedding [13], then scan the sequence from two directions. In [34], a quadri-directional scanning mechanism is proposed to supersede Mamba’s initial 1D scan operation to 2D scan. Subsequent work [4, 23, 24, 30, 41, 61, 66] introduce various scanning methods to explore variations of Mamba in visual representations. However, these works have primarily leveraged the efficiency of the Mamba architecture from an encoder perspective, while its application in the decoder remains relatively constrained. Besides, while benefiting from the efficiency of the Mamba architecture, its application in wide-FoV dense prediction tasks remains unexplored. Therefore, for the first time, we propose a mamba-based decoder to address wide-FoV image segmentation.

3. Methodology

3.1. Overall Architecture

An overview of our Deformable Mamba architecture is presented in Fig. 3, which illustrates how we make Mamba-based models deformable and available for wide-FoV semantic segmentation. It mainly follows the Encoder-Decoder architecture. The backbone selection is flexible for different methods like CNN-, Transformer- or Mamba-based architectures. In this work, we explore with VMamba [34] as the backbone and our proposed Deformable Mamba Decoder. In our framework, there are two model sizes: DMamba-M (Mini) and DMamba-T (Tiny).

Specifically, given the wide-FoV input image of shape $H \times W \times 3$, a stem module is firstly utilized to patchify the original image into the shape of $\frac{H}{4} \times \frac{W}{4} \times 3$, the encoder gradually down-samples feature maps in the l^{th} stage with channel dimensions $C_l \in \{96, 192, 384, 768\}$ and resolutions $R_l \in \{\frac{H}{4} \times \frac{W}{4}, \frac{H}{8} \times \frac{W}{8}, \frac{H}{16} \times \frac{W}{16}, \frac{H}{32} \times \frac{W}{32}\}$. These features are hierarchically fused in our proposed Deformable Mamba Decoder. The output features from the decoder’s final layer are first processed through a fully connected layer and subsequently transformed via feature channel convolutions to generate the predicted semantic map.

3.2. Deformable Mamba Decoder

The Deformable Mamba Decoder comprises four efficient fusion and upsampling modules. Within this framework, we propose a novel **Deformable Mamba Fusion (DMF)** block, which effectively integrates multi-scale features while enabling the decoder to adaptively process distorted data. Considering the diverse types and degrees of distortion present in different wide-FoV data, our method is not tailored to any specific dataset. Instead, we incorporate distortion awareness into the model in a simple, broadly applicable manner.

As shown in lower part of Fig. 3, the DMF block takes two inputs, E_i and D_j , where E_i represents the multi-scale

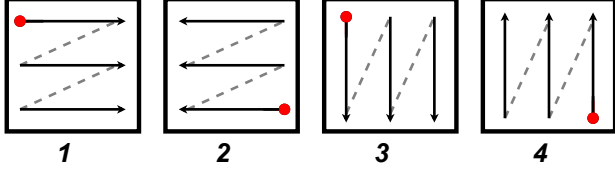


Figure 4. For an embedded 2D sequence, Mamba [17] employs a uni-directional scan from start to end (1). [72] utilizes a bi-directional scan combining (1) and (2), while [34] adopts a quadri-directional scanning incorporating (1), (2), (3), and (4).

feature maps output by the encoder, and D_j denotes the features fused by the DMF block. Here, indices i and j range from 1 to 4 and 0 to 3, respectively, following the constraint $i + j = 4$. Specifically, for the first stage of DMF block, both inputs are derived from the feature maps of the last encoder layer, *i.e.*, $E_4 = D_0$. To maximize efficiency by minimizing decoder computational complexity, we employ only a single quadri-directional scanning layer, originally introduced in the 2D selective scan (SS2D) block by Liu *et al.* [34] for embedding feature D_j into the state space.

We posit that enabling model distortion-aware capability hinges on providing the model with sufficient deformable capacity, thereby endowing the model with the intrinsic ability to adaptively learn and generalize from distorted data representations. Deformable Convolutions (DCNs) [11, 53, 56, 74] render the rigid kernels in conventional convolution more flexible and dynamically adaptive by introducing data-dependent offsets, which allows the fixed sampling locations to be dynamically adjusted based on the data. [75] provides the Transformer-based model with a data-driven receptive field, enabling the model’s perception of image distortions and deformations. SSM, which describes the dynamics of a system, can be formulated as:

$$\begin{aligned} \mathbf{h}'(\mathbf{t}) &= \mathbf{A}\mathbf{h}(\mathbf{t}) + \mathbf{B}\mathbf{x}(\mathbf{t}), \\ \mathbf{y}(\mathbf{t}) &= \mathbf{C}\mathbf{h}(\mathbf{t}), \end{aligned} \quad (1)$$

where $\mathbf{x}(\mathbf{t})$ and $\mathbf{y}(\mathbf{t})$ denote the inputs and outputs of the system, respectively, $\mathbf{h}(\mathbf{t})$ is the inner states of the system, \mathbf{A} , \mathbf{B} , \mathbf{C} are the system parameters.

Mamba [17] and its visual variants [4, 23, 24, 30, 34, 41, 61, 66, 72] are based on SSM. As shown in Fig. 4, while methods such as [4, 72] have attempted to model the spatial information of images by expanding scanning paths, the inherent one-by-one token processing makes it more challenging to integrate a learnable deformation mechanism into state-space modeling, compared to CNN- and Transformer-based architectures. To address this, we adopt a compromise solution by following [64, 65, 68], we incorporate deformable convolution to augment the model’s deformable capacity. In particular, we feed the encoder feature E_i into one single DCNv2 [74] layer with a kernel size of 3×3 ,

which can be mathematically formulated as follows:

$$\mathbf{E}_{\text{out}}(\mathbf{p}) = \sum_{k=1}^K \mathbf{w}_k \mathbf{m}_k \mathbf{E}_{\text{in}}(\mathbf{p} + \mathbf{p}_k + \Delta \mathbf{p}_k), \quad (2)$$

where \mathbf{p} represents the current location in feature map, \mathbf{w}_k and \mathbf{p}_k denote the weight and initial offsets for the k -th location, respectively. The parameter \mathbf{m}_k is a learnable modulation scalar that modulates the input feature amplitudes from different spatial locations. In our implementation, $\mathbf{K} = 9$ and $\mathbf{p}_k \in (-1, -1), \dots, (1, 1)$ defines a 3×3 convolutional kernel with dilation 1.

The outputs from both branches, each with dimensions $\{h \times w \times c\}$, are concatenated to form a tensor with dimensions $\{h \times w \times 2c\}$, which is subsequently processed by an upsampling module. To fully preserve the feature information from both branches while endowing the model with additional learnable capacity, we refrain from employing parameter-free upsampling methods such as bilinear interpolation. Instead, after an initial feature fusion via a series of 3×3 convolutions, we enhance the resolution of feature maps using the Pixelshuffle [46] operation, which can be formulated as:

$$\mathcal{PS}(T)_{h,w,2c} = T_{2h,2w,\frac{c}{2}}, \quad (3)$$

where \mathcal{PS} is an periodic shuffling operator that rearranges the elements of a input tensor T from shape $\{h \times w \times 2c\}$ to $\{2h \times 2w \times \frac{c}{2}\}$.

The upsampled features are linearly projected as the output of the DMF block. Uniquely, the feature map in the final stage, after undergoing convolutional fusion, is not subjected to the PixelShuffle operation for channel reduction and resolution enhancement. It is worth noting that in all the experiments presented in Sec. 4, the decoder architecture is kept consistent, with no dataset-specific modifications. The only adjustment made is to the final output layer, which is tailored to accommodate the varying semantic categories across the datasets.

Our Deformable Mamba Decoder leverages the advantages of the Mamba architecture’s linear computational complexity, resulting in superior computational efficiency. Simultaneously, it addresses the challenge that Mamba, in contrast to CNNs and Transformers, lacks the architectural ability to provide deformation awareness at the feature level. Besides, we introduce distortion awareness exclusively from the decoder perspective, decoupling it from the overall framework and thus enhancing the model’s flexibility and adaptability. Comprehensive qualitative and quantitative analyses in Sec. 4 showcase the exceptional performance and efficiency of our decoder.

4. Experiment Results

To validate our deformable Mamba method, we compare with state-of-the-art approaches on three 360° panoramic and two 180° fisheye datasets. Additionally, we conduct experiments using CNN-, Transformer-, and Mamba-based architectures (e.g., ResNet, Swin, VMamba) to validate the efficiency and effectiveness of our Deformable Mamba Decoder.

4.1. Datasets

Stanford2D3D [1] consists of 1,413 indoor 360° images with a resolution of 512×1024, encompassing 13 distinct object categories.

Matterport3D [3] has 10,615 indoor 360° images. Following [21, 50], 7,829 of panoramas with a resolution of 1024×2048 are used for training and 772 for evaluation.

SynPASS [65] is a synthetic outdoor 360° dataset from CARLA [14]. It contains 9,080 images with a resolution of 1024×2048, covering various weather conditions (cloudy, foggy, rainy, sunny) and illumination (daytime, nighttime).

WoodScape [62] consists of 10K 180° images captured by four surround view cameras. The semantic labels have 9 categories. Since the test split is not available, 8,234 released images are reallocated into training and evaluation sets with an 80% to 20% split.

SynWoodScape [45] is a synthetic version of the surround-view dataset. The released v0.1.1 version contains 2,000 180° surround-view fisheye RGB images. We split them into training and validation sets with an 80% to 20% ratio.

4.2. Implementation Details

In this work, our models are trained and validated on three 360° datasets and two 180° datasets, covering both indoor and outdoor scenarios, as well as real and synthetic environments, using 4 A100 GPUs. For all experiments, we employed cross-entropy as the loss function. To validate the effectiveness of our framework, we deliberately avoided using any auxiliary losses. The models were optimized using AdamW with an initial learning rate of $6e^{-5}$ and weight decay of 0.01. For Stanford2D3D and SynWoodScape, we trained for 80K iterations with a batch size of 2 per GPU. For Matterport3D, SynPASS, and WoodScape, we extended the training to 160K iterations, maintaining the same batch size of 2 per GPU. The learning rate schedule consisted of a linear warm-up for the first 1.5K iterations, followed by a polynomial decay with a power of 0.9.

4.3. Effectiveness and Robustness analysis

Adaptability to different backbones. As mentioned in Sec. 1 and Sec. 3, decoupling the deformable setting from the overall framework and introducing it exclusively from the decoder perspective somewhat reduces the model’s capability to perceive distortions in wide-FoV data. The ad-

Table 1. **Results on Stanford2D3D**, using **ResNet-50** [22] as the backbone with 23.5M parameters, 22.9G FLOPs and hierarchical embedding dimensions of {256, 512, 1024, 2048}.

Decoder	Params (M) ↓	FLOPs (G) ↓	Results ↑	
			mIoU	Acc
UperHead [54] (CVPR20)	40.5	250.7	53.34	62.42
MusterHead [57] (CVPR21)	203.1	211.5	54.39	63.27
CGRHead [38] (CVPR23)	282.6	31.4	54.12	62.94
Ours	77.3	38.8	57.22	66.32

Table 2. **Results on Stanford2D3D**, using **Swin-T** [35] as the backbone with 27.5M parameters, 25.6G FLOPs and hierarchical embedding dimensions of {96, 192, 384, 768}.

Decoder	Params (M) ↓	FLOPs (G) ↓	Results ↑	
			mIoU	Acc
UperHead [54] (CVPR20)	31.5	206.9	53.82	63.06
MusterHead [57] (CVPR21)	19.1	21.4	52.36	54.54
CGRHead [38] (CVPR23)	40.6	5.0	54.26	62.90
Ours	11.2	6.0	55.09	65.30

Table 3. **Results on Stanford2D3D**, using **VMamba-T** [34] as the backbone with 29.5M parameters, 25.3G FLOPs and hierarchical embedding dimensions of {96, 192, 384, 768}.

Decoder	Params (M) ↓	FLOPs (G) ↓	Results ↑	
			mIoU	Acc
UperHead [54] (CVPR20)	31.5	206.9	56.80	65.01
MusterHead [57] (CVPR21)	19.1	21.4	58.12	66.97
CGRHead [38] (CVPR23)	40.6	5.0	56.45	65.07
Ours	11.2	6.0	59.30	68.99

vantage, however, lies in enhancing the model’s flexibility. Through the plug-in distortion-aware decoder, we enable the model to adaptively perceive image deformations for different backbones. On the Stanford2D3D panoramic dataset, we compared our Deformable Mamba Decoder with UperHead [54], MusterHead [57], CGRHead [38], evaluating their adaptability to CNN-, Transformer-, and Mamba-based backbones. As shown in Tables 1, 2, and 3, compared to decoders lacking distortion perception, our method achieves the best performance across ResNet-50 [22], Swin-T [35], and VMamba-T [34] backbones, which demonstrates the significance of distortion perception for wide-FoV image understanding.

Efficiency of the decoder. We emphasize that an efficient decoder is crucial for alleviating the overall model complexity. For instance, Liu *et al.* utilize UperHead as the decoder to evaluate VMamba’s application in semantic segmentation tasks. As shown in Table 3, with VMamba as the backbone, the model has only 25.3G FLOPs, while the decoder UperHead, with 206.9G FLOPs, becomes the bottleneck of the models’ computational complexity. While MusterHead and CGRHead reduce computational complexity, they exhibit strong sensitivity to the model scale. As evidenced in Table 1, their parameter count experiences substantial growth with increasing embedding dimensions. In contrast, our proposed decoder showcases superior compatibility with diverse model scales while retaining lower tem-

poral and spatial complexity.

Based on the results, our method provides substantial distortion-aware capability for CNN-, Transformer-, and Mamba-based models while maintaining excellent efficiency, demonstrating its adaptability and robustness.

4.4. Qualitative Results

Visualization of distortion-aware capability. To showcase the distortion-aware capability of our decoder, we present a visual comparison against UperHead [54] lacking deformable design on the 360° Stanford2D3D and 180° SynWoodScape datasets. As shown in Fig. 5, the baseline model struggles to accurately segment narrow and elongated areas such as door frames, vegetation contours, traffic light poles, and lane markings. In contrast, our proposed DMamba with Deformable Mamba Decoder effectively addresses these challenges, significantly improving segmentation performance on small and elongated objects.

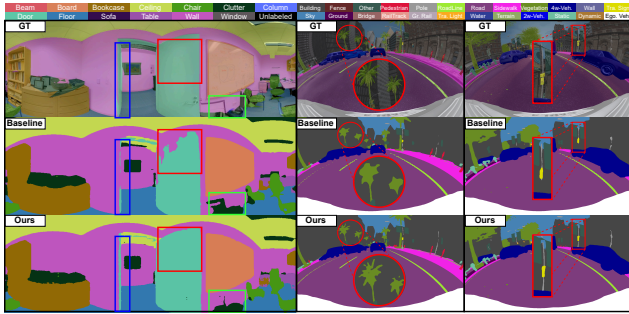
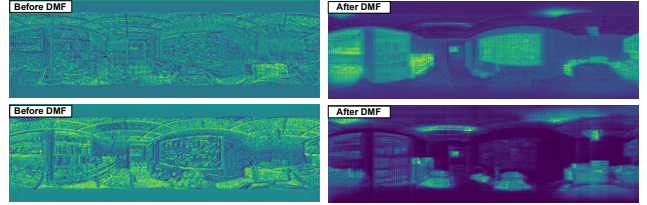


Figure 5. Visualization of the wide-FoV segmentation results. From left to right: one 360° and two 180° segmentation.

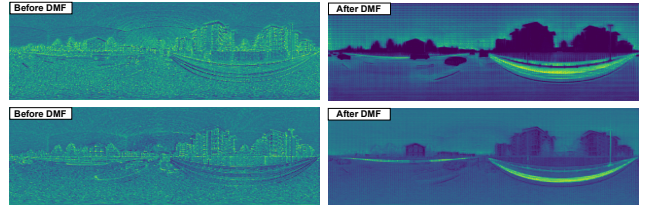
Analysis of feature maps. As shown in Figure 6, to illustrate how the DMF module enhances distortion awareness, we visualize the channel map extracted from the encoder and the corresponding output features of DMF block. Specifically, we present the results of channels #6 and #68 in the second layer of the first decoder stage. Prior to passing through the DMF block, the features primarily focus on global structures while lacking adequate emphasis on crucial regions such as small objects in cluttered indoor environments 6a or severely distorted areas in wide-FoV outdoor scenes 6b. Without explicit distortion-aware adaptation, the feature representation remains less effective in preserving fine-grained spatial details and compensating for geometric distortions. The model shows enhanced attention to objects at different scales after traversing the DMF block.

4.5. Quantitative Results

We extensively evaluate our proposed method across the five aforementioned datasets, addressing the critical challenge of data heterogeneity prevalent in existing methods. Through meticulous comparative experiments with



(a) Visualization of feature maps in indoor scenarios



(b) Visualization of feature maps in outdoor scenarios

Figure 6. **Visualization of feature maps.** From left to right: features extracted by Mamba-based encoder (**Before DMF**) and features fused by the DMF module (**After DMF**). Effective detection and recognition of small objects in indoor scenarios (a), such as pictures on walls, requires the model to exhibit enhanced local perception capabilities. In contrast, outdoor scenarios (b) captured by wide-FoV cameras are often characterized by significant object deformation and distortion. To facilitate accurate scene understanding in such cases, the model must be equipped with a robust ability to handle and perceive distortion effectively.

Table 4. **Results on 360° segmentation datasets** of Stanford2D3D (S2D3D) fold-1 and 360FV-Matterport (MP3D). †denotes our re-implementation.

Method	Backbone	mIoU	
		S2D3D	MP3D
Tangent [15] (CVPR20)	ResNet-101	45.6	-
HoHoNet [48] (CVPR21)	ResNet-101	52.0	44.1
CBFC [71] (CVPR23)	ResNet-101	52.2	-
Trans4PASS [64] (CVPR22)	Trans4PASS	52.1	41.9
Trans4PASS+ [65] (PAMI24)	Trans4PASS+	54.0	42.6
SegFormer [55] (NeurIPS21)	MiT-B2	51.9	45.5
360BEV [50] (WACV24)	MiT-B2	54.3	46.3
SGAT4PASS [31] (IJCAI23)	MiT-B2	56.4	-
360SFUDA† [70] (CVPR24)	MixT-B2	54.9	46.7
360SFUDA† [70] (CVPR24)	MixT-B3	56.9	47.9
SegNeXt† [20] (NeurIPS22)	MSCAN-B	57.0	48.4
VMamba† [34] (NeurIPS24)	VMamba-T	56.8	47.6
DMamba-M (Ours)	VMamba-T	59.3	48.7
DMamba-T (Ours)	VMamba-S	60.2	49.3

state-of-the-art approaches and a careful re-implementation of [20, 70], we systematically investigate the performance variations induced by diverse data distributions and types, thereby providing comprehensive insights into model generalizability and robustness.

Results on 360° Stanford2D3D dataset. Table 4 shows superior performance of our method compared to both distortion-aware [15, 31, 48, 50, 64, 65, 70, 71] and

Table 5. **Results on 360° segmentation dataset** SynPASS. †denotes our re-implementation.

Method	mIoU	Building	Fence	Other	Pedestrian	Pole	RoadLine	Road	SideWalk	Vegetation	Vehicles	Wall	TrafficSign	Sky	Ground	Bridge	RailTrack	GroundRail	TrafficLight	Static	Dynamic	Water	Terrain
PVT-T [52] (CVM22)	32.37	74.83	19.94	00.24	21.82	13.15	62.59	93.14	49.09	67.27	46.44	01.69	09.63	96.09	00.18	02.64	08.81	61.11	14.09	12.04	00.99	05.05	51.33
PVT-S [52] (CVM22)	32.68	78.02	27.12	00.27	23.48	16.51	59.81	92.87	50.21	66.22	43.50	01.12	08.67	96.34	00.44	00.15	02.82	63.88	13.78	15.15	01.58	08.78	48.29
SegFormer-B1 [55] (NeurIPS21)	37.36	78.24	20.59	00.00	38.28	21.09	68.72	94.50	59.72	68.43	67.51	00.83	09.86	96.08	00.56	01.38	20.79	69.59	23.38	19.91	01.38	08.97	52.07
SegFormer-B2 [55] (NeurIPS21)	37.24	79.25	23.58	00.00	40.01	20.14	65.28	92.80	46.92	68.64	77.45	01.42	15.00	96.33	00.57	00.58	02.68	67.60	25.89	20.80	01.99	20.92	51.53
Trans4PASS-T [64] (CVPR22)	38.53	79.17	28.18	00.13	36.04	23.69	69.16	95.51	61.71	69.77	71.12	01.53	16.98	96.50	00.56	01.60	15.22	70.48	26.03	23.11	02.08	09.24	49.77
Trans4PASS-S [64] (CVPR22)	38.57	80.02	24.56	00.07	41.49	25.23	72.00	95.89	59.88	69.07	77.08	01.04	13.72	96.69	00.67	00.73	05.60	72.56	25.93	22.45	02.78	08.34	52.65
Trans4PASS+(T) [65] (PAMI24)	39.42	79.63	24.45	00.21	44.23	26.71	70.32	95.86	61.80	69.25	78.85	01.09	13.81	97.12	00.91	03.48	19.32	72.44	21.08	25.56	02.67	05.03	53.20
Trans4PASS+(S) [65] (PAMI24)	40.72	80.91	20.78	00.23	45.36	24.08	72.51	96.79	67.15	70.46	81.39	04.28	26.19	97.21	01.24	01.74	16.56	67.08	28.64	23.68	03.35	08.48	57.57
SegNeXt-B† [20] (NeurIPS22)	39.90	82.62	16.06	00.12	43.21	26.15	71.69	97.10	60.64	67.56	82.56	00.32	24.43	97.23	02.03	00.00	43.23	47.90	31.61	26.50	03.63	10.56	42.68
360SFUDA-B2† [70] (CVPR24)	40.37	82.69	22.27	00.16	41.86	28.19	74.98	97.13	62.22	70.05	81.55	04.21	21.09	97.45	01.06	00.49	31.77	51.08	32.15	24.88	03.59	10.02	49.23
360SFUDA-B3† [70] (CVPR24)	41.33	82.91	32.33	00.23	41.87	27.21	75.13	97.37	62.90	69.34	82.95	01.66	26.03	97.56	00.95	00.10	41.39	64.02	32.30	26.74	03.48	16.76	48.14
DMamba-M(Ours)	41.72	83.19	21.52	00.21	48.15	32.20	75.8	97.51	61.00	67.74	81.86	01.06	31.30	94.47	01.37	00.68	29.63	49.41	36.35	30.99	04.08	20.54	45.27
DMamba-T(Ours)	42.78	84.24	22.57	00.25	49.20	33.25	76.85	98.56	62.05	68.79	82.91	02.11	32.35	98.52	02.42	01.73	30.68	50.46	37.40	32.04	05.85	21.59	46.32

non-distortion-aware [20, 34] methods. Specifically, our DMamba-M model with the VMamba-T as backbone achieves a significant mIoU improvement of +2.9% to +13.7% over panoramic baselines. Notably, compared to the VMamba [54], our lightweighted decoder with the same backbone achieves a +2.5% higher mIoU while reducing overall parameters by 20% and FLOPs by 86%. Furthermore, our DMamba-T model, which has a comparable parameter count to VMamba, demonstrates even better performance with a +3.4% mIoU improvement.

Results on 360° Matterport3D dataset. While our DMamba-M demonstrates remarkable performance on Stanford2D3D dataset, the challenge becomes more pronounced on large-scale Matterport3D panoramic datasets, where we observe a relatively modest improvement margin of +0.3% mIoU over the previous SOTA model SegNeXt as shown in Table 4. Remarkably, our DMamba-T achieves more substantial gains of +0.9% and +1.7% mIoU compared to SegNeXt and VMamba-T respectively, with comparable model capacities.

Results on 360° SynPASS dataset. Beyond real-world datasets, we evaluate the generalizability of our method on synthetic and outdoor scenes on the 360° SynPASS dataset. It is worth noting that despite SegNeXt’s superior performance over 360SFUDA in real-world scenarios, it exhibits a substantial performance degradation on the synthetic dataset. This discrepancy underscores the sensitivity of certain architectures to data distribution shifts. In contrast, our method, as shown in Table 5, achieves the state-of-the-art mIoU of 42.78%, surpassing all existing panoramic and pinhole-based methods. Explicitly, our DMamba-T overall achieves top scores on *pedestrian*, *pole*, *traffic sign*, *static* and *dynamic*. For *traffic sign* with slender properties, our model enjoys more than +6.0% mIoU.

Results on 180° WoodScape dataset. In Table 6, we present a comparison of our method with other models us-

Table 6. **Results on 180° segmentation dataset** WoodScape. †denotes our re-implementation.

Method	Mutli-task	Supervised	mIoU
MeanTeacher [49] (NeurIPS17)	✗	✗	54.20
CPS [8] (CVPR21)	✗	✗	60.31
CPS with CutMix [8] (CVPR21)	✗	✗	62.47
FishSegSSL [40] (J. Imaging24)	✗	✗	64.81
OmniDet [29] (RA-L21)	✗	✓	72.50
+ DTP [19] (ECCV18)	✓	✓	75.80
+ GradNorm [9] (PMLR18)	✓	✓	75.90
+ Uncertainty [27] (CVPR18)	✓	✓	76.10
+ VarNorm [29] (RA-L21)	✓	✓	76.60
SegNeXt-B† [20] (NeurIPS22)	✗	✓	82.32
360SFUDA-B2† [70] (CVPR24)	✗	✓	81.74
360SFUDA-B3† [70] (CVPR24)	✗	✓	82.43
DMamba-M (Ours)	✗	✓	83.21
DMamba-T (Ours)	✗	✓	83.90

Table 7. **Results on 180° segmentation dataset** SynWoodScape. †denotes our re-implementation.

Method	mIoU
SegNeXt-B† [20] (NeurIPS22)	64.86
360SFUDA-B2† [70] (CVPR24)	66.56
360SFUDA-B3† [70] (CVPR24)	67.47
DMamba-M (Ours)	69.20
DMamba-T (Ours)	69.62

ing 180° fisheye inputs from the WoodScape dataset [62]. Semi-supervised methods such as MeanTeacher [49], CPS [8], and FishSegSSL [40] show lower performance due to the limited data. Compared to multi-task models, our proposed DMamba, designed with deformable settings, outperforms all variants of the OmniDet [29] model. Although SegNeXt and 360SFUDA perform well on the WoodScape dataset, our method, with a more compact architecture still achieves a higher mIoU by +0.9% and +0.8%, respectively. The DMamba-T variant further advances the state-

of-the-art mIoU to 83.9%, confirming DMamba’s effectiveness in capturing heavily distorted object information in wide-FoV segmentation.

Results on 180° SynWoodScape dataset. Due to the lack of baseline comparisons on SynWoodScape, we limited our evaluation to SegNeXt and 360SFUDA. As shown in Table 7, similar to the results on SynPASS, SegNeXt and 360SFUDA perform similarly on real 180° datasets, while the former exhibits a significant performance degradation on synthetic data. This further confirms the challenge of achieving consistently high performance when data distribution shifts. In comparison, our DMamba-M of similar scale outperforms them by +4.36% and +1.73% mIoU, respectively, achieving an improved segmentation accuracy of 69.20 mIoU on SynWoodScape.

These consistent improvements across all five wide-FoV datasets demonstrate the effectiveness of our proposed framework in unifying wide-FoV segmentation.

4.6. Ablation Study

To further analyze the effect of different components on our proposed framework, we conduct ablation study on the Stanford2D3D dataset.

Analysis of scanning mechanism. To ensure consistency, we adopt the same scanning method as in [34], as our model primarily uses its Mamba-based encoder. As mentioned in Sec. 1, the SSM-based Mamba processes input tokens sequentially, which is suitable for textual data. However, for image data, where tokens have spatial relationships, multi-directional scanning is more appropriate. To highlight the difference between various scanning methods on our framework, we conducted ablation experiments on the Stanford2D3D dataset. As shown in Table 8, both uni-directional scanning and bi-directional scanning results in slight performance drop.

Table 8. Analysis of scanning methods.

Scan Method	mIoU	mAcc
Uni-direction	57.53	67.52
Bi-direction	57.94	67.66
Quadri-direction (Ours)	59.30	68.99

Study of defomable convolution. In Sec. 1 and Sec. 2, we outlined the limitations of tightly coupling deformable designs with the entire model and the challenges faced by Mamba-based models in integrating deformable mechanisms due to their sequential processing of input tokens. We propose to introduce sufficient distortion awareness into the model by paralleling DCN in the decoder and integrating it through feature fusion. We replace deformable convolution with traditional one as shown in Table 9, the results prove the effectiveness of this trade-off solution.

Table 9. Ablation Study of deformable designs.

Deformable	mIoU	mAcc
✗	57.45	66.52
✓	59.30 (+1.85%)	68.99 (+2.47%)

Analysis of upsampling methods. Sampling methods play a critical role in our approach. As mentioned earlier, our decoder utilizes two branches to achieve complete feature modeling and the incorporation of distortion awareness respectively. To optimize computational efficiency, we adopt a single-layer module in each branch, which reduces model complexity while limiting the model’s learnable capacity. As a result, we disregard parameter-free interpolation-based upsampling methods, opting instead to fuse features from both branches and employ periodic arrangement to preserve all information. In Table 10, we compare bilinear and bicubic methods, showing the importance of our design.

Table 10. Analysis of upsample methods.

Upsample Method	mIoU	mAcc
Bilinear Interpolation	56.90	66.08
Bicubic Interpolation	56.97	66.12
PixelShuffle (Ours)	59.30	68.99

5. Conclusion

In this work, we are the first to explore the unification of the wide field of view (FoV) segmentation tasks, including 180° and 360° image segmentation. Most existing models are tailored for pinhole camera images, making it challenging to extend their success to wide-FoV domains due to the severe image distortion and object deformation. We incorporate the model’s distortion-aware capability exclusively from the decoder perspective, decoupling it from the overall architecture to enhance flexibility and facilitate seamless integration with various model architectures. Consistent improvements across five diverse wide-FoV datasets, ranging from indoor to outdoor, from synthetic to real-world scenes, demonstrate that our method effectively addresses the unique challenges of wide-FoV segmentation.

Limitations and Future Work. Given the rapid advancement of Large Language Models (LLMs), integrating multi-modal LLMs presents a promising direction for future research. Their strong generalization capabilities and semantic understanding could significantly enhance our unified semantic segmentation framework, particularly in handling diverse wide-FoV segmentation tasks. This integration could bridge the gap between linguistic semantic understanding and geometric feature learning, potentially leading to more robust and versatile segmentation models.

References

- [1] I Armeni. Joint 2d-3d semantic data for indoor scene understanding. *arXiv preprint arXiv:1702.01105*, 2017. 1, 2, 5
- [2] Vijay Badrinarayanan, Alex Kendall, and Roberto Cipolla. Segnet: A deep convolutional encoder-decoder architecture for image segmentation. *IEEE transactions on pattern analysis and machine intelligence*, 39(12):2481–2495, 2017. 1, 2
- [3] Angel Chang, Angela Dai, Thomas Funkhouser, Maciej Halber, Matthias Niessner, Manolis Savva, Shuran Song, Andy Zeng, and Yinda Zhang. Matterport3d: Learning from rgb-d data in indoor environments. *arXiv preprint arXiv:1709.06158*, 2017. 1, 2, 5
- [4] Keyan Chen, Bowen Chen, Chenyang Liu, Wenyuan Li, Zhengxia Zou, and Zhenwei Shi. Rsmamba: Remote sensing image classification with state space model. *IEEE Geoscience and Remote Sensing Letters*, 2024. 2, 3, 4
- [5] Liang-Chieh Chen, Yukun Zhu, George Papandreou, Florian Schroff, and Hartwig Adam. Encoder-decoder with atrous separable convolution for semantic image segmentation. In *Proceedings of the European conference on computer vision (ECCV)*, pages 801–818, 2018. 1, 2
- [6] Shoufa Chen, Enze Xie, Chongjian Ge, Runjian Chen, Ding Liang, and Ping Luo. Cyclemlp: A mlp-like architecture for dense prediction. *arXiv preprint arXiv:2107.10224*, 2021. 2
- [7] Shoufa Chen, Enze Xie, Chongjian Ge, Runjian Chen, Ding Liang, and Ping Luo. Cyclemlp: A mlp-like architecture for dense visual predictions. *IEEE Transactions on Pattern Analysis and Machine Intelligence*, 45(12):14284–14300, 2023. 1
- [8] Xiaokang Chen, Yuhui Yuan, Gang Zeng, and Jingdong Wang. Semi-supervised semantic segmentation with cross pseudo supervision. In *Proceedings of the IEEE/CVF conference on computer vision and pattern recognition*, pages 2613–2622, 2021. 7
- [9] Zhao Chen, Vijay Badrinarayanan, Chen-Yu Lee, and Andrew Rabinovich. Gradnorm: Gradient normalization for adaptive loss balancing in deep multitask networks. In *International conference on machine learning*, pages 794–803. PMLR, 2018. 7
- [10] Bowen Cheng, Alex Schwing, and Alexander Kirillov. Pixel classification is not all you need for semantic segmentation. *Advances in neural information processing systems*, 34:17864–17875, 2021. 2
- [11] Jifeng Dai, Haozhi Qi, Yuwen Xiong, Yi Li, Guodong Zhang, Han Hu, and Yichen Wei. Deformable convolutional networks. In *Proceedings of the IEEE international conference on computer vision*, pages 764–773, 2017. 4
- [12] Liuyuan Deng, Ming Yang, Hao Li, Tianyi Li, Bing Hu, and Chunxiang Wang. Restricted deformable convolution-based road scene semantic segmentation using surround view cameras. *IEEE Transactions on Intelligent Transportation Systems*, 21(10):4350–4362, 2019. 3
- [13] Alexey Dosovitskiy. An image is worth 16x16 words: Transformers for image recognition at scale. *arXiv preprint arXiv:2010.11929*, 2020. 3
- [14] Alexey Dosovitskiy, German Ros, Felipe Codevilla, Antonio Lopez, and Vladlen Koltun. Carla: An open urban driving simulator. In *Conference on robot learning*, pages 1–16. PMLR, 2017. 5
- [15] Marc Eder, Mykhailo Shvets, John Lim, and Jan-Michael Frahm. Tangent images for mitigating spherical distortion. In *Proceedings of the IEEE/CVF Conference on Computer Vision and Pattern Recognition*, pages 12426–12434, 2020. 6
- [16] Jun Fu, Jing Liu, Haijie Tian, Yong Li, Yongjun Bao, Zhiwei Fang, and Hanqing Lu. Dual attention network for scene segmentation. In *Proceedings of the IEEE/CVF conference on computer vision and pattern recognition*, pages 3146–3154, 2019. 2
- [17] Albert Gu and Tri Dao. Mamba: Linear-time sequence modeling with selective state spaces. *arXiv preprint arXiv:2312.00752*, 2023. 2, 3, 4
- [18] Jiaqi Gu, Hyoukjun Kwon, Dilin Wang, Wei Ye, Meng Li, Yu-Hsin Chen, Liangzhen Lai, Vikas Chandra, and David Z Pan. Multi-scale high-resolution vision transformer for semantic segmentation. In *Proceedings of the IEEE/CVF conference on computer vision and pattern recognition*, pages 12094–12103, 2022. 2
- [19] Michelle Guo, Albert Haque, De-An Huang, Serena Yeung, and Li Fei-Fei. Dynamic task prioritization for multitask learning. In *Proceedings of the European conference on computer vision (ECCV)*, pages 270–287, 2018. 7
- [20] Meng-Hao Guo, Cheng-Ze Lu, Qibin Hou, Zhengning Liu, Ming-Ming Cheng, and Shi-Min Hu. Segnext: Rethinking convolutional attention design for semantic segmentation. *Advances in Neural Information Processing Systems*, 35:1140–1156, 2022. 1, 2, 6, 7
- [21] Suresh Guttikonda and Jason Rambach. Single frame semantic segmentation using multi-modal spherical images. In *Proceedings of the IEEE/CVF Winter Conference on Applications of Computer Vision*, pages 3222–3231, 2024. 5
- [22] Kaiming He, Xiangyu Zhang, Shaoqing Ren, and Jian Sun. Deep residual learning for image recognition. In *Proceedings of the IEEE conference on computer vision and pattern recognition*, pages 770–778, 2016. 5
- [23] Vincent Tao Hu, Stefan Andreas Baumann, Ming Gui, Olga Grebenkova, Pingchuan Ma, Johannes Fischer, and Bjorn Ommer. Zigma: Zigzag mamba diffusion model. *arXiv preprint arXiv:2403.13802*, 2024. 3, 4
- [24] Tao Huang, Xiaohuan Pei, Shan You, Fei Wang, Chen Qian, and Chang Xu. Localmamba: Visual state space model with windowed selective scan. *arXiv preprint arXiv:2403.09338*, 2024. 2, 3, 4
- [25] Zilong Huang, Xinggang Wang, Lichao Huang, Chang Huang, Yunchao Wei, and Wenyu Liu. Ccnet: Criss-cross attention for semantic segmentation. In *Proceedings of the IEEE/CVF international conference on computer vision*, pages 603–612, 2019. 2
- [26] Alexander Jaus, Kailun Yang, and Rainer Stiefelhagen. Panoramic panoptic segmentation: Towards complete surrounding understanding via unsupervised contrastive learning. In *2021 IEEE Intelligent Vehicles Symposium (IV)*, pages 1421–1427. IEEE, 2021. 2

- [27] Alex Kendall, Yarin Gal, and Roberto Cipolla. Multi-task learning using uncertainty to weigh losses for scene geometry and semantics. In *Proceedings of the IEEE conference on computer vision and pattern recognition*, pages 7482–7491, 2018. 7
- [28] Alex Krizhevsky, Ilya Sutskever, and Geoffrey E Hinton. Imagenet classification with deep convolutional neural networks. *Advances in neural information processing systems*, 25, 2012. 3
- [29] Varun Ravi Kumar, Senthil Yogamani, Hazem Rashed, Ganesh Sitsu, Christian Witt, Isabelle Leang, Stefan Milz, and Patrick Mäder. Omnidet: Surround view cameras based multi-task visual perception network for autonomous driving. *IEEE Robotics and Automation Letters*, 6(2):2830–2837, 2021. 1, 3, 7
- [30] Kunchang Li, Xinhao Li, Yi Wang, Yinan He, Yali Wang, Limin Wang, and Yu Qiao. Videomamba: State space model for efficient video understanding. *arXiv preprint arXiv:2403.06977*, 2024. 2, 3, 4
- [31] Xuewei Li, Tao Wu, Zhongang Qi, Gaoang Wang, Ying Shan, and Xi Li. Sgat4pass: spherical geometry-aware transformer for panoramic semantic segmentation. *arXiv preprint arXiv:2306.03403*, 2023. 6
- [32] Zechao Li, Yanpeng Sun, Liyan Zhang, and Jinhui Tang. Ctnet: Context-based tandem network for semantic segmentation. *IEEE Transactions on Pattern Analysis and Machine Intelligence*, 44(12):9904–9917, 2021. 2
- [33] Yazhou Liu, Yuliang Chen, Pongsak Lasang, and Qunsun Sun. Covariance attention for semantic segmentation. *IEEE Transactions on Pattern Analysis and Machine Intelligence*, 44(4):1805–1818, 2020. 2
- [34] Yue Liu, Yunjie Tian, Yuzhong Zhao, Hongtian Yu, Lingxi Xie, Yaowei Wang, Qixiang Ye, and Yunfan Liu. Vmamba: Visual state space model. *arXiv preprint arXiv:2401.10166*, 2024. 1, 2, 3, 4, 5, 6, 7, 8
- [35] Ze Liu, Yutong Lin, Yue Cao, Han Hu, Yixuan Wei, Zheng Zhang, Stephen Lin, and Baining Guo. Swin transformer: Hierarchical vision transformer using shifted windows. In *Proceedings of the IEEE/CVF international conference on computer vision*, pages 10012–10022, 2021. 5
- [36] Jonathan Long, Evan Shelhamer, and Trevor Darrell. Fully convolutional networks for semantic segmentation. In *Proceedings of the IEEE conference on computer vision and pattern recognition*, pages 3431–3440, 2015. 2
- [37] Anam Manzoor, Aryan Singh, Ganesh Sistu, Reenu Mohandas, Eoin Grua, Anthony Scanlan, and Ciarán Eising. Deformable convolution based road scene semantic segmentation of fisheye images in autonomous driving. In *IET Conference Proceedings CP887*, pages 7–14. IET, 2024. 3
- [38] Zhenliang Ni, Xinghao Chen, Yingjie Zhai, Yehui Tang, and Yunhe Wang. Context-guided spatial feature reconstruction for efficient semantic segmentation. *arXiv preprint arXiv:2405.06228*, 2024. 2, 5
- [39] Sneha Paul, Zachary Patterson, and Nizar Bouguila. Semantic segmentation using transfer learning on fisheye images. In *2023 International Conference on Machine Learning and Applications (ICMLA)*, pages 445–452. IEEE, 2023. 3
- [40] Sneha Paul, Zachary Patterson, and Nizar Bouguila. Fish-segssl: A semi-supervised semantic segmentation framework for fish-eye images. *Journal of Imaging*, 10(3):71, 2024. 3, 7
- [41] Xiaohuan Pei, Tao Huang, and Chang Xu. Efficientvmamba: Atrous selective scan for light weight visual mamba. *arXiv preprint arXiv:2403.09977*, 2024. 3, 4
- [42] Clément Ployon, Ola Ahmad, Freddy Lecue, and Farida Cheriet. Adaptable deformable convolutions for semantic segmentation of fisheye images in autonomous driving systems. *arXiv preprint arXiv:2102.10191*, 2021. 3
- [43] Tran Minh Quan, David Grant Colburn Hildebrand, and Won-Ki Jeong. Fusionnet: A deep fully residual convolutional neural network for image segmentation in connectomics. *Frontiers in Computer Science*, 3:613981, 2021. 3
- [44] Olaf Ronneberger, Philipp Fischer, and Thomas Brox. U-net: Convolutional networks for biomedical image segmentation. In *Medical image computing and computer-assisted intervention—MICCAI 2015: 18th international conference, Munich, Germany, October 5–9, 2015, proceedings, part III 18*, pages 234–241. Springer, 2015. 3
- [45] Ahmed Rida Sekkat, Yohan Dupuis, Varun Ravi Kumar, Hazem Rashed, Senthil Yogamani, Pascal Vasseur, and Paul Honeine. Synwoodscape: Synthetic surround-view fisheye camera dataset for autonomous driving. *IEEE Robotics and Automation Letters*, 7(3):8502–8509, 2022. 1, 2, 5
- [46] Wenzhe Shi, Jose Caballero, Ferenc Huszár, Johannes Totz, Andrew P Aitken, Rob Bishop, Daniel Rueckert, and Zehan Wang. Real-time single image and video super-resolution using an efficient sub-pixel convolutional neural network. In *Proceedings of the IEEE conference on computer vision and pattern recognition*, pages 1874–1883, 2016. 4
- [47] Robin Strudel, Ricardo Garcia, Ivan Laptev, and Cordelia Schmid. Segmenter: Transformer for semantic segmentation. In *Proceedings of the IEEE/CVF international conference on computer vision*, pages 7262–7272, 2021. 1, 2
- [48] Cheng Sun, Min Sun, and Hwann-Tzong Chen. Hohonet: 360 indoor holistic understanding with latent horizontal features. In *Proceedings of the IEEE/CVF Conference on Computer Vision and Pattern Recognition*, pages 2573–2582, 2021. 6
- [49] Antti Tarvainen and Harri Valpola. Mean teachers are better role models: Weight-averaged consistency targets improve semi-supervised deep learning results. *Advances in neural information processing systems*, 30, 2017. 1, 7
- [50] Zhifeng Teng, Jiaming Zhang, Kailun Yang, Kunyu Peng, Hao Shi, Simon Reiß, Ke Cao, and Rainer Stiefelhagen. 360bev: Panoramic semantic mapping for indoor bird’s-eye view. In *Proceedings of the IEEE/CVF Winter Conference on Applications of Computer Vision*, pages 373–382, 2024. 5, 6
- [51] A Vaswani. Attention is all you need. *Advances in Neural Information Processing Systems*, 2017. 3
- [52] Wenhai Wang, Enze Xie, Xiang Li, Deng-Ping Fan, Kaitao Song, Ding Liang, Tong Lu, Ping Luo, and Ling Shao. Pvt v2: Improved baselines with pyramid vision transformer. *Computational Visual Media*, 8(3):415–424, 2022. 7

- [53] Wenhai Wang, Jifeng Dai, Zhe Chen, Zhenhang Huang, Zhiqi Li, Xizhou Zhu, Xiaowei Hu, Tong Lu, Lewei Lu, Hongsheng Li, et al. Internimage: Exploring large-scale vision foundation models with deformable convolutions. In *Proceedings of the IEEE/CVF conference on computer vision and pattern recognition*, pages 14408–14419, 2023. 4
- [54] Tete Xiao, Yingcheng Liu, Bolei Zhou, Yuning Jiang, and Jian Sun. Unified perceptual parsing for scene understanding. In *Proceedings of the European conference on computer vision (ECCV)*, pages 418–434, 2018. 2, 5, 6, 7
- [55] Enze Xie, Wenhai Wang, Zhiding Yu, Anima Anandkumar, Jose M Alvarez, and Ping Luo. Segformer: Simple and efficient design for semantic segmentation with transformers. *Advances in neural information processing systems*, 34: 12077–12090, 2021. 1, 2, 6, 7
- [56] Yuwen Xiong, Zhiqi Li, Yuntao Chen, Feng Wang, Xizhou Zhu, Jiapeng Luo, Wenhai Wang, Tong Lu, Hongsheng Li, Yu Qiao, et al. Efficient deformable convnets: Rethinking dynamic and sparse operator for vision applications. In *Proceedings of the IEEE/CVF Conference on Computer Vision and Pattern Recognition*, pages 5652–5661, 2024. 4
- [57] Jing Xu, Wentao Shi, Pan Gao, Zhengwei Wang, and Qizhu Li. Uperformer: A multi-scale transformer-based decoder for semantic segmentation. *arXiv preprint arXiv:2211.13928*, 2022. 2, 5
- [58] Chenhongyi Yang, Zehui Chen, Miguel Espinosa, Linus Ericsson, Zhenyu Wang, Jiaming Liu, and Elliot J Crowley. Plainmamba: Improving non-hierarchical mamba in visual recognition. *arXiv preprint arXiv:2403.17695*, 2024. 2
- [59] Kailun Yang, Xinxin Hu, Luis M Bergasa, Eduardo Romera, Xiao Huang, Dongming Sun, and Kaiwei Wang. Can we pass beyond the field of view? panoramic annular semantic segmentation for real-world surrounding perception. In *2019 IEEE Intelligent Vehicles Symposium (IV)*, pages 446–453. IEEE, 2019. 2
- [60] Kailun Yang, Xinxin Hu, Luis M Bergasa, Eduardo Romera, and Kaiwei Wang. Pass: Panoramic annular semantic segmentation. *IEEE Transactions on Intelligent Transportation Systems*, 21(10):4171–4185, 2019. 2
- [61] Yijun Yang, Zhaohu Xing, and Lei Zhu. Vivim: a video vision mamba for medical video object segmentation. *arXiv preprint arXiv:2401.14168*, 2024. 3, 4
- [62] Senthil Yogamani, Ciarán Hughes, Jonathan Horgan, Ganesh Sistu, Padraig Varley, Derek O’Dea, Michal Uricár, Stefan Milz, Martin Simon, Karl Amende, et al. Woodscape: A multi-task, multi-camera fisheye dataset for autonomous driving. In *Proceedings of the IEEE/CVF International Conference on Computer Vision*, pages 9308–9318, 2019. 1, 2, 5, 7
- [63] Yuhui Yuan, Lang Huang, Jianyuan Guo, Chao Zhang, Xilin Chen, and Jingdong Wang. Ocnet: Object context for semantic segmentation. *International Journal of Computer Vision*, 129(8):2375–2398, 2021. 2
- [64] Jiaming Zhang, Kailun Yang, Chaoxiang Ma, Simon Reiß, Kunyu Peng, and Rainer Stiefelhagen. Bending reality: Distortion-aware transformers for adapting to panoramic semantic segmentation. In *Proceedings of the IEEE/CVF conference on computer vision and pattern recognition*, pages 16917–16927, 2022. 1, 2, 4, 6, 7
- [65] Jiaming Zhang, Kailun Yang, Hao Shi, Simon Reiß, Kunyu Peng, Chaoxiang Ma, Haodong Fu, Philip HS Torr, Kaiwei Wang, and Rainer Stiefelhagen. Behind every domain there is a shift: Adapting distortion-aware vision transformers for panoramic semantic segmentation. *IEEE Transactions on Pattern Analysis and Machine Intelligence*, 2024. 1, 2, 4, 5, 6, 7
- [66] Zeyu Zhang, Akide Liu, Ian Reid, Richard Hartley, Bohan Zhuang, and Hao Tang. Motion mamba: Efficient and long sequence motion generation. In *European Conference on Computer Vision*, pages 265–282. Springer, 2025. 3, 4
- [67] Junwei Zheng, Jiaming Zhang, Kailun Yang, Kunyu Peng, and Rainer Stiefelhagen. Materobot: Material recognition in wearable robotics for people with visual impairments. In *2024 IEEE International Conference on Robotics and Automation (ICRA)*, pages 2303–2309. IEEE, 2024. 1, 2
- [68] Junwei Zheng, Ruiping Liu, Yufan Chen, Kunyu Peng, Chengzhi Wu, Kailun Yang, Jiaming Zhang, and Rainer Stiefelhagen. Open panoramic segmentation. In *European Conference on Computer Vision*, pages 164–182. Springer, 2025. 2, 4
- [69] Sixiao Zheng, Jiachen Lu, Hengshuang Zhao, Xiatian Zhu, Zekun Luo, Yabiao Wang, Yanwei Fu, Jianfeng Feng, Tao Xiang, Philip HS Torr, et al. Rethinking semantic segmentation from a sequence-to-sequence perspective with transformers. In *Proceedings of the IEEE/CVF conference on computer vision and pattern recognition*, pages 6881–6890, 2021. 1, 2
- [70] Xu Zheng, Pengyuan Zhou, Athanasios V Vasilakos, and Lin Wang. Semantics distortion and style matter: Towards source-free uda for panoramic segmentation. In *Proceedings of the IEEE/CVF Conference on Computer Vision and Pattern Recognition*, pages 27885–27895, 2024. 2, 6, 7
- [71] Zishuo Zheng, Chunyu Lin, Lang Nie, Kang Liao, Zhijie Shen, and Yao Zhao. Complementary bi-directional feature compression for indoor 360deg semantic segmentation with self-distillation. In *Proceedings of the IEEE/CVF Winter Conference on Applications of Computer Vision*, pages 4501–4510, 2023. 6
- [72] Lianghui Zhu, Bencheng Liao, Qian Zhang, Xinlong Wang, Wenyu Liu, and Xinggang Wang. Vision mamba: Efficient visual representation learning with bidirectional state space model. *arXiv preprint arXiv:2401.09417*, 2024. 2, 3, 4
- [73] Qinfeng Zhu, Yuanzhi Cai, Yuan Fang, Yihan Yang, Cheng Chen, Lei Fan, and Anh Nguyen. Samba: Semantic segmentation of remotely sensed images with state space model. *Heliyon*, 10(19), 2024. 2
- [74] Xizhou Zhu, Han Hu, Stephen Lin, and Jifeng Dai. Deformable convnets v2: More deformable, better results. In *Proceedings of the IEEE/CVF conference on computer vision and pattern recognition*, pages 9308–9316, 2019. 4
- [75] Xizhou Zhu, Weijie Su, Lewei Lu, Bin Li, Xiaogang Wang, and Jifeng Dai. Deformable detr: Deformable transformers for end-to-end object detection. *arXiv preprint arXiv:2010.04159*, 2020. 4